Quantum Electronics **51** (3) 201–205 (2021) ©2021 Kvantovaya Elektronika and IOP Publishing Limited

https://doi.org/10.1070/QEL17445

Type-II GaAsBi QDs/GaSb for middle-wave and long-wave infrared lasers

Zhongyue Zhang, Liyao Zhang, Mingxuan Zhang, Shuang Yao, Peng Yu, Xiaodan Li

Abstract. **A GaSb/GaAsBi type-II quantum dot structure is proposed for fabricating middle-wave infrared (MWIR) and long-wave infrared (LWIR) lasers. The finite element method is employed to investigate the train distributions and band structures of the proposed structures with different Bi contents and QD sizes. It is found that the strain component ε_{xx} decreases with Bi contents and heights, and increases with the diameter, while the component ε_{zz} inversely changes. The charge carriers recombine between the electrons in GaAsBi QDs and the holes in GaSb. The energy of the ground states of electrons of GaAsBi QDs decreases and the emission wavelength increases with the Bi contents and QD sizes. The emission wavelength can cover MWIR and LWIR ranges with proper Bi contents and QD sizes. The proposed structure provides a feasible way to fabricate MWIR and LWIR lasers.**

Keywords: *GaAsBi quantum dot, type-II structure, infrared lasers.*

1. Introduction

GaAsBi is a member of the dilute bismides, which is formed by incorporating a small amount of Bi atoms into GaAs. GaAsBi was first realised by MOVPE in 1998 [1] and by MBE in 2003 [2]. Since the successful synthesis, GaAsBi has attracted extensive attentions due to its remarkable properties. With every 1% of Bi incorporated into GaAsBi, its bandgap is reduced by 60–90 meV [2–4]. In the meanwhile, the spin–orbit splitting energy of GaAsBi increases with Bi content [5]. When the Bi content is over 10%, the spin–orbit splitting energy is even larger than the bandgap [6], which significantly reduces the Auger recombination. Moreover, the bandgap of GaAsBi is expected to be temperature insensitive because it consists of semiconductor and semimetal components [7]. These properties make GaAsBi a potential candidate in the application in optoelectronic devices operating in the infrared region [8]. Recent years, several GaAsBi-based devices have been successfully fabricated. The first optically pumped GaAsBi laser was realised in 2010 [9], and the first electrically pumped GaAsBi laser was fabricated in 2013 [10]. The longest emission wavelength of the reported GaAsBi laser is 1.407 μm [11], operating in the short-wave infrared (SWIR) region. A further increase in the Bi content can increase the emission wavelength to middle-wave infrared (MWIR) and long-wave infrared (LWIR) regions. However, it is difficult to incorporate a high content of Bi for almost all kinds of dilute bismides [12–16]. Moreover, high Bi incorporation always requires low temperature growth [17], which deteriorates the optical property of the material. The reported highest Bi content in GaAsBi thin films is 22% [17], while the reported GaAsBi lasers make use of GaAsBi thin films or quantum wells as an active region, with the Bi content varying from 2.5% to 6%. A moderate Bi content is preferred for fabricating GaAsBi-based lasers [9–11, 18–22]. Nowadays, the most popular MWIR (3–5 μm) and LWIR (8–14 μm) lasers are quantum cascade lasers (QCLs) and interband cascade lasers (ICLs), fabricated with antimonides and/or arsenides [23–25]. The structures of QCLs and ICLs are complex and intricate [26]. Fine control is needed for the material growth of QCLs and ICLs.

In this work, we propose a GaSb/GaAsBi type-II quantum dot (QD) structure. The strain distributions and band structures are calculated by the finite element method (FEM). The emission wavelength from MWIR to LWIR regions can be achieved through the control of the Bi contents and QD sizes. The required Bi content is low, which solves the problems for high Bi incorporations and the accompanying deteriorating optical properties. In the meanwhile, the quantum confine effect of the QD can effectively improve the light emission efficiency. The proposed structure is simple and easy to realise. The proposed structure provides a feasible way to fabricate infrared lasers, operating in MWIR and LWIR regions.

2. Methods

Figure 1a shows a three-dimensional schematic diagram of the proposed GaSb/GaAsBi QD structure. The thicknesses of the lower and upper GaSb layers are 50 nm each. The GaAsBi QD is assumed to have a dome shape. The Bi contents M, the diameter D and the height H of the QD vary from 0 to 11%, from 10 nm to 40 nm, and from 1 nm to 10 nm, respectively. The strain distributions are calculated using continuum elasticity theory [27]. The stress tensor σ and strain tensor ε have the form

$$\sigma = \begin{bmatrix} \sigma_{xx} & \sigma_{xy} & \sigma_{xz} \\ \sigma_{yx} & \sigma_{yy} & \sigma_{yz} \\ \sigma_{zx} & \sigma_{zy} & \sigma_{zz} \end{bmatrix}, \quad \varepsilon = \begin{bmatrix} \varepsilon_{xx} & \varepsilon_{xy} & \varepsilon_{xz} \\ \varepsilon_{yx} & \varepsilon_{yy} & \varepsilon_{yz} \\ \varepsilon_{zx} & \varepsilon_{zy} & \varepsilon_{zz} \end{bmatrix}. \quad (1)$$

According to Hooke's law, the relationship between σ and ε is

Zhongyue Zhang, Liyao Zhang, Mingxuan Zhang, Shuang Yao, Peng Yu, Xiaodan Li Department of Physics, University of Shanghai for Science and Technology, 200093 Shanghai, China;
e-mail: lyzhang@usst.edu.cn

Received 21 September 2020; revision received 23 November 2020
Kvantovaya Elektronika **51** (3) 201–205 (2021)
Submitted in English

$$\sigma_y = \sum_{k=1}^{3}\sum_{l=1}^{3} C_{i,j,k,l}\varepsilon_{kl}, \tag{2}$$

where C is the elastic modulus tensor. Because the off-diagonal elements of σ and ε are symmetrical, formula (2) can be written as

$$\begin{bmatrix}\sigma_{xx}\\ \sigma_{yy}\\ \sigma_{zz}\\ \sigma_{xy}\\ \sigma_{yz}\\ \sigma_{zz}\end{bmatrix} = \begin{bmatrix} C_{11} & C_{12} & C_{13} & C_{14} & C_{15} & C_{16}\\ C_{21} & C_{22} & C_{23} & C_{24} & C_{25} & C_{26}\\ C_{31} & C_{32} & C_{33} & C_{34} & C_{35} & C_{36}\\ C_{41} & C_{42} & C_{43} & C_{44} & C_{45} & C_{46}\\ C_{51} & C_{52} & C_{53} & C_{54} & C_{55} & C_{56}\\ C_{61} & C_{62} & C_{63} & C_{64} & C_{65} & C_{66}\end{bmatrix}\begin{bmatrix}\varepsilon_{xx}\\ \varepsilon_{yy}\\ \varepsilon_{zz}\\ \varepsilon_{xy}\\ \varepsilon_{yz}\\ \varepsilon_{zz}\end{bmatrix}. \tag{3}$$

Because of the symmetry of the zinc-blende structure, C can be simplified as

$$C = \begin{bmatrix} C_{11} & C_{12} & C_{12} & 0 & 0 & 0\\ C_{12} & C_{11} & C_{12} & 0 & 0 & 0\\ C_{12} & C_{12} & C_{11} & 0 & 0 & 0\\ 0 & 0 & 0 & C_{44} & 0 & 0\\ 0 & 0 & 0 & 0 & C_{44} & 0\\ 0 & 0 & 0 & 0 & 0 & C_{44}\end{bmatrix}. \tag{4}$$

After the strain distributions were calculated, the band structure were calculated based on the deformation potential theory [13]. The band alignment and the ground states of electrons and holes are calculated from solving the Schrödinger equation:

$$\left(\frac{-\hbar^2}{m^*}\nabla^2 + V_0 + V_s\right)\varphi(r) = E\varphi(r), \tag{5}$$

where m^* is the effective mass, V_0 is the band offset between GaAsBi and GaSb, and V_s is the strain-induced potential. The strain-induced potentials for the electrons, heavy holes and light holes have the form

$$V_e = a_c(\varepsilon_{xx} + \varepsilon_{yy} + \varepsilon_{zz}), \tag{6}$$

$$V_{hh} = -P - Q, \tag{7}$$

$$V_{lh} = -P + [Q - \Delta + (\Delta^2 + 2Q\Delta + 9Q^2)^{1/2}]/2, \tag{8}$$

where

$$P = -a_v(\varepsilon_{xx} + \varepsilon_{yy} + \varepsilon_{zz}), \tag{9}$$

$$Q = -b(\varepsilon_{xx} + \varepsilon_{yy} - 2\varepsilon_{zz})/2, \tag{10}$$

a_c and a_v are the hydrostatic deformation potentials for the conduction band (CB) and valence band (VB), respectively; b is the shear deformation potential; and Δ is the spin–orbit splitting energy. The parameters used in this paper are listed in Table 1. The lattice constants of GaAs, GaBi, and GaSb are

Table 1. Parameters used for calculations.

Parameters	GaAs [28]	GaBi	GaSb [28]
C_{11}/GPa	1221	81.6 [32]	884.2
C_{12}/GPa	566	28.1 [32]	402.6
C_{44}/GPa	600	59.7 [32]	432.2
a_c/eV	–7.17		–7.5
a_v/eV	–1.16		–0.8
b/eV	2.0		–2.0
Δ/eV	0.341	2.15[31]	0.76
m_e^*	$0.063m_0$	$0.0655m_0$ [33]	$0.041m_0$
m_{hh}^*	$0.51m_0$	$1.23m_0$ [33]	$0.4m_0$
m_{lh}^*	$0.082m_0$	$0.18m_0$ [33]	$0.05m_0$

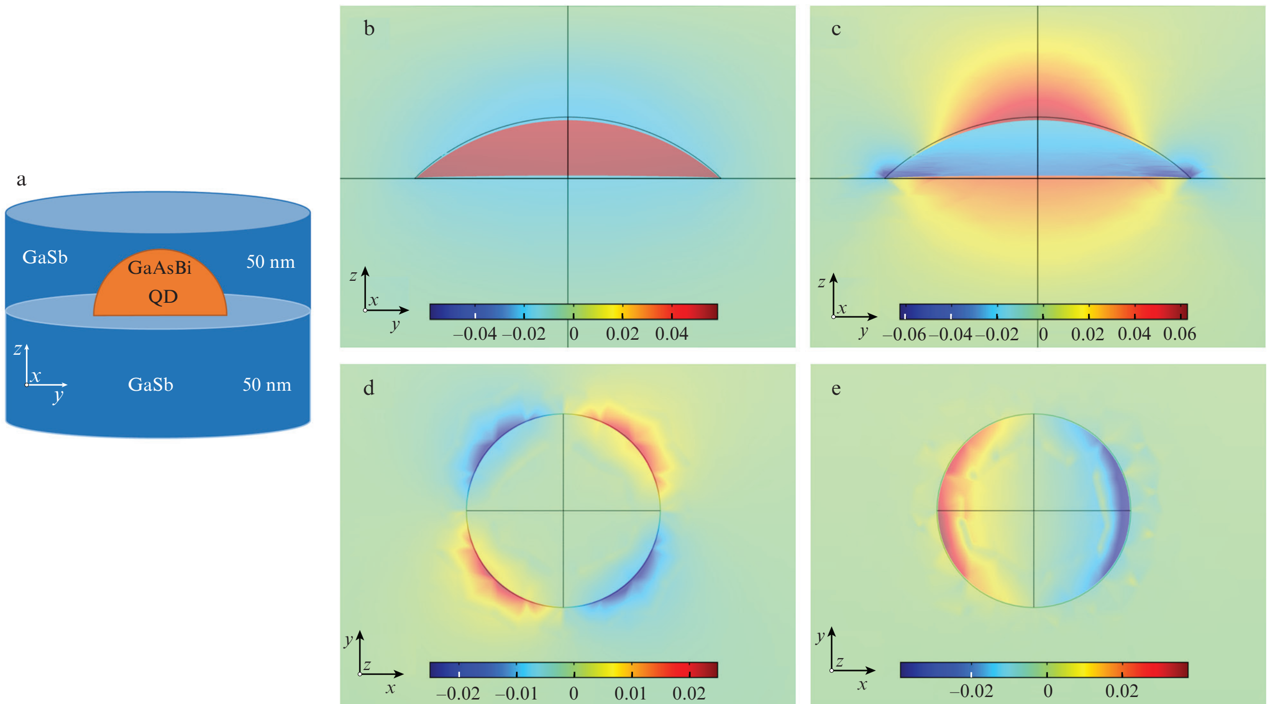

Figure 1. (Colour online) (a) Schematic diagram of a two-dimensional structure of a GaSb/GaAsBi QD and strain distribution of (b) ε_{xx} and (c) ε_{zz} in the yz plane and (d) xy and (e) xz in the xy plane for the GaSb/GaAsBi QD structure with M = 6%, D = 20 nm and H = 4 nm.

5.65, 6.32 and 6.10 Å, respectively [28, 29]. The lattice constants and the elastic coefficients C_{11}, C_{12} and C_{44} of GaAsBi are deduced from a linear interpolation from those of GaAs and GaBi. Due to the lack of data, the deformation potentials a_c and a_v of GaAsBi are assumed to be equal to those of GaAs, considering the Bi content is low in the calculations. The value of b for $GaAs_{1-x}Bi_x$ is obtained from the formula $b(\text{GaAs}) - 0.163x$ [30], while Δ of GaAsBi is deduced from a quadratic interpolation from GaAs and GaBi, with a bowing parameter of −6 eV [31].

3. Results and discussions

3.1. Strain analysis

Figures 1b–1e show the strain distribution of the GaSb/GaAsBi QD structure, with the Bi content, diameter and height of the QD being $M = 6\%$, $D = 20$ nm and $H = 4$ nm, respectively. The strain component ε_{xx} in the QD is positive and uniform with an average value of 0.05, indicating a tensile in-plane strain. This is because the lattice constant of GaSb is larger than that of GaAsBi. The stress component ε_{xx} in GaSb is negative and rapidly increases to zero from the GaSb/GaAsBi QD interface. The value of ε_{zz} in the QD is negative with an average value of −0.03, indicating a compressive strain in the z direction. The shear strain components ε_{xy} and ε_{xz} (Figs 1d and 1e) are asymmetric in the ε_{xy} plane with an average value of 3.1E-6 and −6.6E-7, respectively.

The influences of the QD sizes and Bi contents on the strain are further investigated and shown in Fig. 2. The values of ε_{xx} and hydrostatic strains ($\varepsilon_{xx} + \varepsilon_{yy} + \varepsilon_{zz}$) are both positive, while the values of ε_{zz} are negative, with the diameter, the height and the Bi content varying from 10 nm to 40 nm, from 1 nm to 6 nm and from 0 to 11%, respectively. It indicates a tensile in-plane strain and a compressive out-of-plane strain. One can see from Fig. 2a that ε_{xx} increases and ε_{zz} decreases with increasing diameter D, with the variation ratio being the larger the smaller the diameter. It follows from Fig. 2b, ε_{xx}

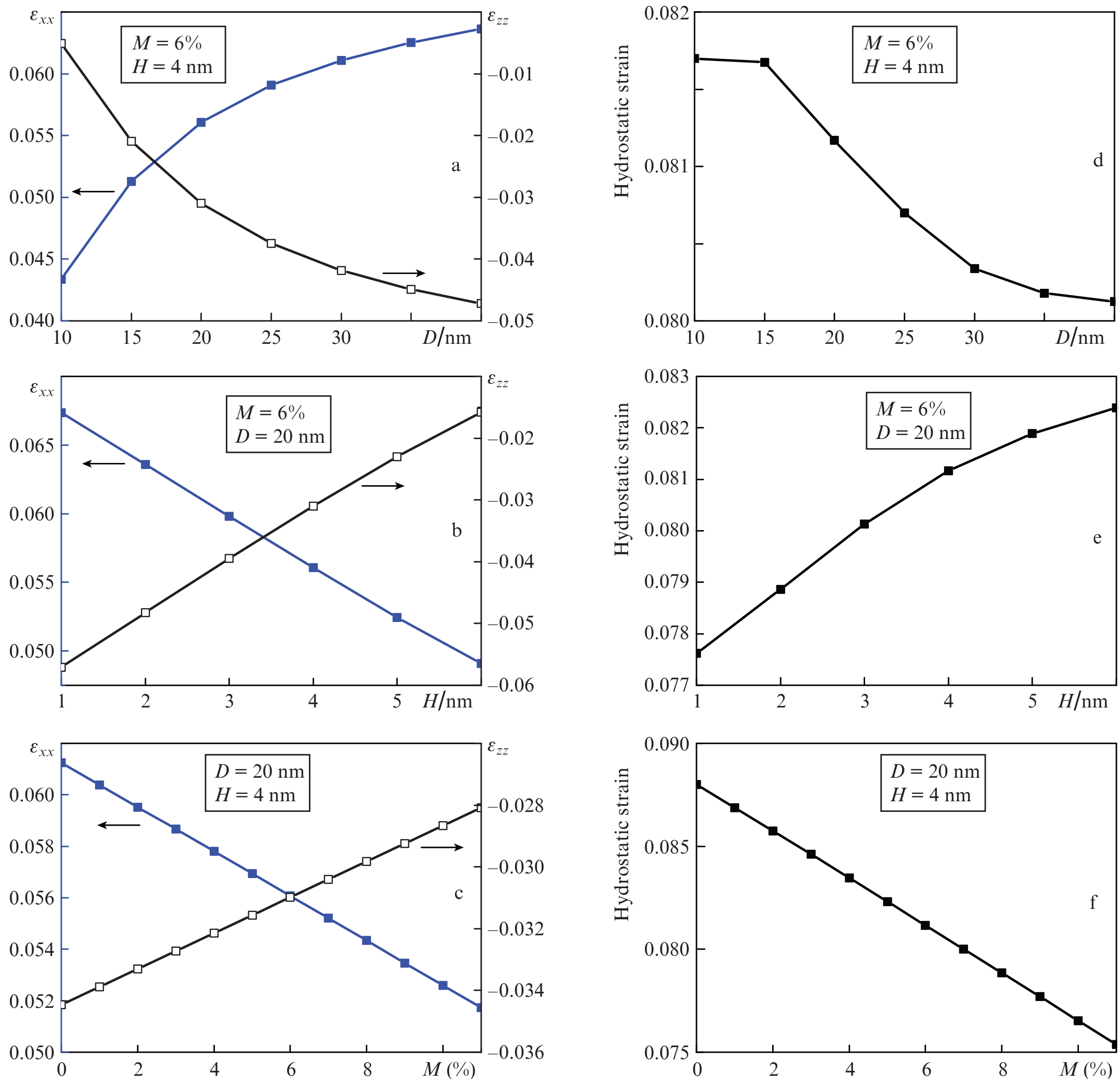

Figure 2. Variations of the strain components ε_{xx} and ε_{zz} in the yz plane with (a) the diameter, (b) height and (c) Bi content, as well as variations of hydrostatic strain with (d) the diameter, (e) height and (f) Bi content of the GaAsBi QD.

decreases monotonously with increasing height H, with a slope of about -0.0035 nm^{-1}, while ε_{zz} increases monotonously with increasing height H, with a slope of about 0.0077 nm^{-1}. In Fig. 2c, the tendency of the variation in ε_{xx} and ε_{zz} with the Bi content M is similar to that with the height H: ε_{xx} decreases linearly with the Bi content, with a slope of $-0.0008/M$, while ε_{zz} increases linearly with the Bi content, with a slope of $0.0005/M$. Figures 2d–2f show the variations of the hydrostatic strains with the QD size and the Bi content: The hydrostatic strain decreases with increasing both D and M and increases with H. The relative variation of the hydrostatic strains with the diameter is much smaller than that with the height and the Bi content.

3.2. Band structure

Figure 3 shows the band alignment of GaSb/GaAsBi QD structure with $M = 6\%$, $D = 20$ nm and $H = 4$ nm. The band alignment is plotted along the z axis across the centre of the GaAsBi QD. A type-II band alignment is formed in this structure. The energy of the valence band maximum of GaSb is set to be zero. Because the thicknesses of the GaSb epi-layers are 50 nm, the light hole band (LHB) and heavy hole band (HHB) of GaSb are still degenerate at the Γ point. The LHB and HHB of GaAsBi QD split, with the LHB above HHB. The charge carriers recombine between the electrons in GaAsBi QD and the holes in GaSb. Because the energy of the valence band maximum of GaSb is set at 0, the radiative recombination energy equals the energy of the ground states of electrons (e1) in GaAsBi QD and is about 0.216 eV, which corresponds to the emission wavelength of about 5.7 μm. This structure can be used for fabricating MWIR lasers.

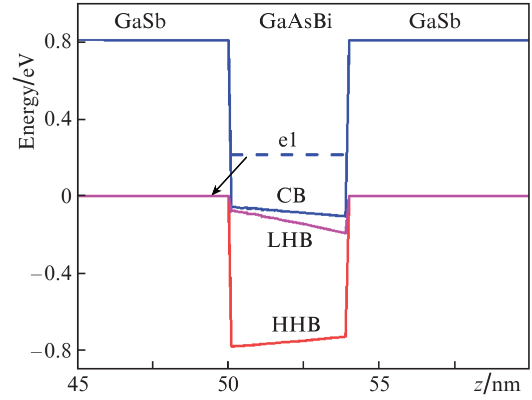

Figure 3. (Colour online) Band alignment of the GaSb/GaAsBi QD structure plotted along the z axis across the centre of the GaAsBi QD, with $M = 6\%$, $D = 20$ nm and $H = 4$ nm, respectively. The blue, red and magnet curves are the conduction band (CB), heavy hole band (HHB) and light hole band (LHB), respectively. The blue dashed line is the ground state of the electrons in the GaAsBi QD. The black arrow shows the carrier recombination in the structure.

The influence of the Bi content and QD size on the band structure and emission wavelength (λ) is shown in Fig. 4, which leads us to conclude that the energy (e1) decreases and the emission wavelength (λ) increases with increasing diameter, height and Bi content, respectively. When the QD diameter increases from 10 nm to 40 nm at $M = 6\%$ and $H = 4$ nm

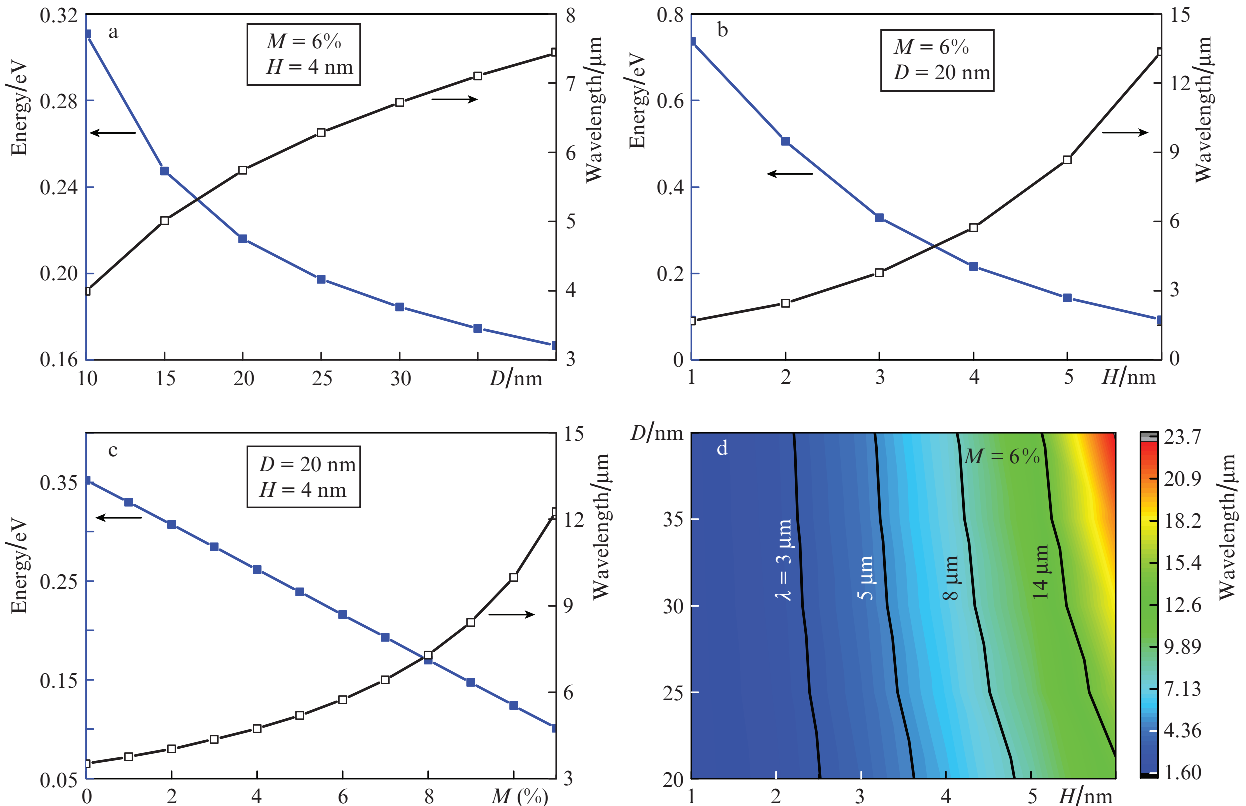

Figure 4. Variations of the ground states of electrons (e1) and the emission wavelength (λ) with (a) the diameter, (b) height and (c) Bi content, as well as (d) two-dimensional mapping of the emission wavelength vs. the diameter and height. The black curves in (d) are the emission wavelength of 3, 5, 8 and 14 μm.

(Fig. 4a), λ increases from 4 to 7.4 µm, corresponding to the MWIR region. In Fig. 4(b), the Bi content and the diameter are 6% and 20 nm, respectively. When the height increases from 1 to 2.4 nm at $M = 6\%$ and $D = 20$ nm, λ increases from 1.7 to 3 µm, corresponding to the short-wave infrared range. When the height increases from 3 nm to 3.6 nm, λ increases from 3.8 µm to 5 µm, corresponding to the MWIR region. When the height increases from 4.8 to 6 nm, λ increases from 8 to 13.4 µm, corresponding to the LWIR region. When the Bi content increases from 0 to 4.5% at $D = 20$ nm and $H =$ 4 nm (Fig. 4 c), λ increases from 3.5 to 5 µm, corresponding to the MWIR region, and when the Bi content increase from 8.6% to 11%, λ increases from 8 to 12.3 µm, corresponding to the LWIR region. Figure 3d shows the variations of λ with the diameter and height, at a fixed Bi content of 6%. The black curves are the proper QD sizes for emitting light at 3, 5, 8 and 14 µm, respectively, i.e. the proper QD sizes for the GaSb/GaAsBi type-II QD structure with a Bi content of 6% to fabricate the MWIR and LWIR lasers. The required Bi content is only 6%, which is easy to be achieved in GaAsBi, with both good structural and optical properties. With the control of Bi contents and QD sizes, the proposed structure can provide a feasible way to fabricate MWIR and LWIR lasers.

4. Conclusions

In this paper, we have proposed a GaSb/GaAsBi type-II QD structure to fabricate MWIR and LWIR lasers. Strain distributions and band structures are investigated with different Bi contents and QD sizes. The GaAsBi QDs generate tensile in-plane strains and compressive out-of-plane strains. The strain components ε_{xx} decreases and ε_{zz} increases increasing with QD diameter, height and Bi content. The hydrostatic strain decreases with both the QD diameter and Bi content, while increases with the QD height. The ground states of electrons in GaAsBi QD decreases while the emission wavelength increases with the QD diameter, height and Bi content. The emission wavelength of the proposed structure can cover MWIR and LWIR regions with proper QD sizes and Bi contents. This structure provides a feasible way to fabricate the MWIR and LWIR lasers.

Acknowledgements. The authors acknowledge supports by the National Natural Science Foundation of China (Grant No. 61904106) and Shanghai Sailing Program (Grant No. 19YF1435300).

References

1. Oe K., Okamoto H. *Jpn. J. Appl. Phys., Pt. 2-Lett.*, **37** (11A), L1283 (1998).
2. Francoeur S., Seong M.J., Mascarenhas A., et al. *Appl. Phys. Lett.*, **82**, 3874 (2003).
3. Tixier S., Adamcyk M., Tiedje T., et al. *Appl. Phys. Lett.*, **82**, 2245 (2003).
4. Alberi K., Dubon O.D., Walukiewicz W., et al. *Appl. Phys. Lett.*, **91**, 051909 (2007).
5. Sweeney S.J., Jin S.R. *J. Appl. Phys.*, **113**, 043110 (2013).
6. Broderick C.A., Usman M., Sweeney S.J., et al. *Semicond. Sci. Technol.*, **27** (9), 094011 (2012).
7. Moussa I., Fitouri H., Rebey A., et al. *Thin Solid Films*, **516** (23), 8372 (2008).
8. Fitouri H., Chakir K., Chine Z., et al. *Mater. Lett.*, **152**, 298 (2015).
9. Tominaga Y., Oe K., Yoshimoto M. *Appl. Phys. Express*, **3** (6), 062201 (2010).
10. Ludewig P., Knaub N., Hossain N., et al. *Appl. Phys. Lett.*, **102**, 242115 (2013).
11. Liu X., Wang L., Fang X., et al. *Photon. Res.*, **7**, 508 (2019).
12. Baladés N., Sales D.L., Herrera M., et al. *Nanoscale Res. Lett.*, **13**, 125 (2018).
13. Zhang L., Song Y., Gong Q. *Int. J. Mol. Sci.*, **20**, 6001 (2019).
14. Pan W., Zhang L., Zhu L., et al. *Semicond. Sci. Technol.*, **32**, 1 (2016).
15. Pan W., Zhang L., Zhu L., et al. *J. Appl. Phys.*, **120**, 094011 (2016).
16. Pan W., Wang P., Wu X., et al. *J. Alloys Compd.*, **656**, 777 (2016).
17. Lewis R.B., Masnadi-Shirazi M., Tiedje T. *Appl. Phys. Lett.*, **101** (8), 963 (2012).
18. Zhou T., Liu X., Cui Y., et al. *AIP Adv.*, **8**, 075306 (2018).
19. Fuyuki T., Yoshioka R., Yoshida K., et al. *Appl. Phys. Lett.*, **103**, 1 (2013).
20. Butkuté R., Geižutis A., et al. *Electron. Lett.*, **50**, 1155 (2014).
21. Fuyuki T., Yoshida K., Yoshioka R., et al. *Appl. Phys. Express*, **7**, 082101 (2014).
22. Kim H., Guan Y., Babcock S.E., et al. *J. Appl. Phys.*, **123**, 113102 (2018).
23. Christola P., Joullié A., Rodrigueza J.B., et al. *Proc. SPIE*, **5582** (2004).
24. Vurgaftman I., Weih R., Kamp M., et al. *Phys. D: Appl. Phys.*, **48**, 123001 (2015).
25. Borri S., Cumis M.S.D., Viciani S., et al. *Proc. SPIE*, **10939** (2020).
26. Becker S., Gerlach G., Hildebrandt L., et al., in *Proc. Progress in Electromagnetic Research Symposium (PIERS)* (Shanghai, China, 8–11 August, 2016).
27. Grundmann M., Stier O., Bimberg D. *Phys. Rev. B.*, **52** (16), 11969 (1995).
28. Vurgaftman I., Jeyer M., Ram-Mohan L. *J. Appl. Phys.*, **89**, 5815 (2001).
29. Masnadi-Shirazi M., Lewis R.B., Bahrami-Yekta V., et al. *J. Appl. Phys.*, **116**, 223506 (2014).
30. Batool Z., Hild K., Hosea T.J.C., et al. *J. Appl. Phys.*, **111** (11), 2245 (2012).
31. Fluegel B., Francoeur S., Mascarenhas A., et al. *Phys. Rev. Lett.*, **97** (6), 067205 (2006).
32. Ferhat M., Zaoui A. *Phys. Rev. Lett.*, **73** (11), 115107 (2006).
33. Zayan A., Stevens M., Vandervelde T.E. *IEEE 43rd Photovoltaic Specialists Conference (PVSC)* (Portland, OR, 2016) p. 2839.